Full Paper

1 **Tissue-specific metabolic reprogramming during wound induced *de novo***

2 **organ formation in tomato hypocotyl explants**

3

4 **Eduardo Larriba**, Instituto de Bioingeniería, Universidad Miguel Hernández, 03202 Elche,

5   Spain; elarriba@umh.es

6 **Ana Belén Sánchez García**, Instituto de Bioingeniería, Universidad Miguel Hernández,

7   03202 Elche, Spain; ana.sanchezg@umh.es

8 **Cristina Martínez-Andújar**, CEBAS-CSIC, Department of Plant Nutrition, Campus

9   Universitario de Espinardo, 30100 Espinardo, Murcia, Spain; cmandujar@cebas.csic.es

10 **Alfonso Albacete**, CEBAS-CSIC, Department of Plant Nutrition, Campus Universitario de

11   Espinardo, 30100 Espinardo, Murcia, Spain; current address: Institute for Agri-Food

12   Research and Development of Murcia (IMIDA), Department of Plant Production and

13   Agrotechnology, 30150 La Alberca, Murcia, Spain; alfonsoa.albacete@carm.es

14 **José Manuel Pérez-Pérez**, Instituto de Bioingeniería, Universidad Miguel Hernández, 03202

15   Elche, Spain, jmperez@umh.es

16

17 Corresponding author: José Manuel Pérez-Pérez (jmperez@umh.es)

18

19 Word count breakdown: Summary, 175; Introduction, 472; Materials and Methods, 1213;

20   Results, 3921; Discussion, 1384; References, 2007; Fig. Legends, 793.

21

22   Figures: 6   Supporting Information: 13

23

24

25

26 **One-sentence Summary:** Metabolic switch during wound-induced regeneration

Full Paper

27 **SUMMARY**

28

29 • Plants have remarkable regenerative capacity, which allows them to survive tissue damaging
30   after biotic and abiotic stress. Some of the key transcription factors and the hormone
31   crosstalk involved in wound-induced organ regeneration have been extensively studied in
32   the model plant *Arabidopsis thaliana*. However, little is known about the role of metabolism
33   in wound-induced organ regeneration.

34 • Here, we performed detailed transcriptome analysis and targeted metabolomics approach
35   during *de novo* organ formation in tomato hypocotyl explants and found tissue-specific
36   metabolic differences and divergent developmental pathways after wounding.

37 • Our results indicate that callus growth in the apical region of the hypocotyl depends on a
38   specific metabolic switch involving the upregulation of the photorespiratory pathway and
39   the differential regulation of photosynthesis-related genes and of the gluconeogenesis
40   pathway.

41 • The endogenous pattern of ROS accumulation in the apical and basal region of the hypocotyl
42   during the time-course were dynamically regulated, and contributed to tissue-specific
43   wound-induced regeneration.

44 • Our findings provide a useful resource for further investigation on the molecular
45   mechanisms involved in wound-induced organ formation in a crop species such as tomato.

46

47

48 **KEYWORDS**

49 *de novo* root regeneration, *de novo* shoot apical meristem formation, time-course bulk RNA-
50 Seq, photosynthesis, photorespiration, glycolysis/gluconeogenesis, reactive oxygen species
51 (ROS).

Full Paper

INTRODUCTION

Plants have remarkable regenerative capacity, enabling them to either repair damaged tissues or regenerate a lost organ (Ikeuchi et al., 2019). Plants regenerative capacity allows them to overcome tissue damage caused by different environmental insults. Moreover, enhanced plant regeneration capabilities have been frequently used during crop production to increase yield by grafting and pruning without killing the plant, as well as for the clonal propagation of elite genotypes.

The many advantages of *Arabidopsis thaliana* and the wide repertoire of regenerative responses in this species have provided some insight into the molecular mechanisms underlying tissue repair and organ regeneration (Ikeuchi et al., 2016; Ikeuchi et al., 2020). Two broad categories of regenerative models have been established, hereafter referred to as tissue culture-induced regeneration and wound-induced regeneration (Mathew and Prasad, 2021). Key transcription factor families and the hormone crosstalk involved in plant regeneration have been extensively studied in this species (Ibáñez et al., 2020). In metazoans, transcription-factor mediated reprogramming of somatic cells into induced pluripotent stem cells (Takahashi and Yamanaka, 2006) involves a profound metabolic shift from oxidative phosphorylation to glycolytic-dependent energy generation (Panopoulos et al., 2012; Cliff and Dalton, 2017). In addition, rewiring of energetic metabolism in cancer cells has been proven essential for tumor progression (Frezza, 2020). Strikingly, in plant tissue culture-induced regeneration, addition of sugars, amino acids and polyamines to the growing media often influence cellular proliferation and regeneration efficiency, although the precise mechanism by which they act is currently unknown. Ectopic expression of Arabidopsis *WOUND INDUCED DEDIFFERENTIATION1* (*WIND1*) in hypocotyl explants of *Brassica napus* enhanced callus formation and root regeneration, a phenotype that correlated with deregulation of metabolites, such as sucrose, proline, gamma aminobutyric acid or putrescine (Iwase et al., 2018). However, the precise link between the activation of a single transcription factor with non-hormone metabolite accumulation and callus formation and regeneration requires additional investigations.

The 'Micro-Tom' cultivar of tomato (*Solanum lycopersicum* L.) has been recognized as a model for tomato research because it shares some key advantages with Arabidopsis including its small size, short life cycle and easy transformation capability (Shikata and Ezura, 2016). High-efficient targeted gene editing using an optimized CRISPR-Cas9 system (Dahan-Meir et al., 2018) and TILLING collections (Okabe et al., 2013) facilitates the use of reverse genetics

85   approaches. In our previous studies on wound-induced adventitious root (AR) formation in

86   tomato (Alaguero-Cordovilla et al., 2020; Alaguero-Cordovilla et al., 2021), we noticed

87   formation of *de novo* shoot meristems at the cut surface of the hypocotyl after removal of the

88   shoot apex. Here, we performed detailed transcriptome analyses and targeted metabolomics

89   approach during *de novo* organ formation (i.e., adventitious shoots and ARs) in tomato

90   hypocotyl explants, to provide a conceptual framework for the identification of the regulatory

91   mechanisms involved in organ regeneration. The findings of this study reveal the role of

92   metabolism on tissue-specific wound-induced organ formation in tomato.

Full Paper

MATERIALS AND METHODS

Plant material and growth conditions

Seedlings of the tomato cultivar 'Micro-Tom' were grown *in vitro* as described elsewhere (Alaguero-Cordovilla et al., 2021). Hypocotyl explants were obtained after removing the whole root system (2-3 mm above the hypocotyl-root junction) and the shoot apex (just below the cotyledons' petiole) with a sharp scalpel, at the 100-101 growth stages (Feller et al., 1995), hereafter 0 days after excision (dae). Hypocotyl explants were transferred to 120 × 120 mm (length × width) Petri dishes containing 75 mL of standard growing medium (SGM) (Alaguero-Cordovilla et al., 2021), otherwise indicated (**Supplemental Table 1a**).

RNA isolation, library construction and NGS sequencing

For each sample, three to four mm of the apical or the basal regions of the hypocotyl were collected at 0, 1, 4 and 8 dae (denoted as T0, T1, T4, and T8). Three biological replicates, each consisting of 12 apical or basal fragments respectively, were obtained, and immediately frozen in liquid N_2. Total RNA from ~100 mg of powdered tissue that was kept at −80 °C was extracted using Spectrum™ Plant Total RNA Kit (Sigma-Aldrich, USA) and treated with DNAse I (ThermoFisher Scientific, USA). The RNA integrity was confirmed using a 2100 Bioanalyzer (Agilent Technologies, USA). Three sequencing libraries from basal tissues and two sequencing libraries form apical tissues at T0, T1, T4 and T8 were obtained with the TruSeq Stranded RNA Sample Preparation Kit v2 (Illumina, USA). NGS sequencing was carried out by Macrogen (Korea) on an Illumina HiSeq4000 in pair-end mode with 100 cycles of sequencing. Additionally, three NGS libraries were sequenced using the BGISEQ-500 pipeline at BGI Genomics (BGI Tech Solutions, Hong Kong, China), in pair-end mode with 150 cycles of sequencing. The raw NGS reads (SRA number) were pre-processed using Trimmomatic (Bolger et al., 2014) and with FastQC (https://www.bioinformatics.babraham.ac.uk/projects/fastqc/) for quality assessment.

RNA-Seq analysis

The bioinformatics workflow used is shown in **Supplemental Figure 1a**. Briefly, clean RNA-Seq reads were mapped to *Solanum lycopersicum* L. genome build SL4.0 (Hosmani et al., 2019) using STAR 2.7 (Dobin et al., 2013). Assignation of reads to gene models (ITAG4.0 annotation) was performed with featureCounts from the Subread package (Liao et al., 2019). Identification

5

Full Paper

126   of significant transcriptional changes was carried out based on Bayesian estimation of temporal

127   regulation (false discovery rate [FDR] = 0.05) (Aryee et al., 2009) implemented in MeV

128   software package (http://mev.tm4.org/). Read count normalization and differential gene

129   expression analysis were carried out using DESeq2 integrated into Differential Expression and

130   Pathway analysis (iDEP 9.1) web application (Ge et al., 2018). Statistics and read count

131   normalization were indicated in **Supplemental Figure 1b-g**. Differential expressed genes

132   (DEG) were filtered using an FDR < 0.01 and Log_2fold change > < |1|. K-means clustering and

133   principal component analysis were carried out using normalized counts on the iDEP 9.1 web

134   application. Web-tool ShinyGO v0.61 (Ge et al., 2020) was used to perform Gene Ontology

135   (GO) enrichment analysis. ITAG4.0 gene structural annotation was retrieved from Sol

136   Genomics Network (SolGenomics; https://solgenomics.net/). Their putative *Arabidopsis*

137   *thaliana* orthologs were identified using BioMart tool from the Emsembl Plants database

138   (Bolser et al., 2017). Genes were assigned to KEGG metabolic pathways by Reciprocal Best

139   Hit BLAST using GhostKOALA (https://www.kegg.jp/ghostkoala/) and SolGenomics BLAST

140   against ITAG4.0. For heatmap and hierarchical clustering analyses, we used Morpheus

141   (https://software.broadinstitute.org/morpheus) webtool.

142

143   **Gene expression analysis by real-time quantitative PCR**

144   Total RNA from ~100 mg of powdered hypocotyl sections from 14 seedlings at T0, T1, T4 and

145   T8 was extracted in triplicate using Spectrum Plant Total RNA Kit (Sigma–Aldrich, United

146   States) and further processed as described elsewhere (Alaguero-Cordovilla et al., 2021). For

147   real-time quantitative PCR (RT-qPCR), primers amplified 115-205 base pairs of the cDNA

148   sequences of selected genes (**Supplemental Table 1b**). RT-qPCR was performed as previously

149   described (Alaguero-Cordovilla et al., 2021).

150

151   **Macroscopic studies of wound-induced organogenesis**

152   Hypocotyl explants were incubated for 10 to 21 days in SGM supplemented with different

153   compounds (**Supplemental Table 1b**). In all these cases, ARs arising from the hypocotyl were

154   visually scored and periodically annotated. AR emergence was estimated based on the day

155   before the observation of the first AR. Shoot regeneration stages were also scored based on the

156   morphological structures observed in the apical region of the hypocotyl. For photorespiration

157   assays, we applied the treatments on 0.2% agarose droplets (25 µL) at the apical region of the

158   hypocotyl explants; shoot regeneration stages were scored at 17 dae.

159

Full Paper

Cell death and reactive oxygen species (ROS) assays

For microscopic examination of dying cells, hypocotyl explants at T0, T1, T4 and T8 were stained on hot acetic acid/trypan blue solution (0.5% w/v in 45% acetic acid) for 3 minutes. After incubation for 1 hour at room temperature, hypocotyls were cleared in chloral hydrate (80 g chloral hydrate in 30 mL distilled water). For DAB staining, whole hypocotyl explants atT0, T1, T4 and T8 dae were immersed on a 1% (w/v) solution of DAB in Tris-HCl buffer, pH 4.8. After 1 hour of vacuum infiltration, samples were kept in DAB solution overnight at room temperature. Then, explants were cleared in chloral hydrate solution. To confirm the specific accumulation of H_2O_2, before DAB staining, we incubated hypocotyl explants with 100 units·μl^{-1} catalase (Sigma-Aldrich) for 30 minutes. Thereafter, samples were processed as indicated above.

Metabolite extraction and analysis

Three biological replicates, each consisting of eight apical or basal regions of the hypocotyl were collected at T0, T1, T4 and T8. Metabolites were extracted from frozen tissues and were analyzed as described previously by (Albacete et al., 2008) with some modifications. Fresh plant material (0.1 g) was homogenized in liquid nitrogen and incubated in 1 mL of cold (−20 °C) extraction mixture of methanol/water (80/20, v/v) for 30 min at 4 ºC. Solids were separated by centrifugation (20,000 g, 15 min at 4 ºC) and re-extracted for another 30 min at 4 ºC with 1 mL of extraction solution. Pooled supernatants were passed through Sep-Pak Plus C18 cartridges to remove interfering lipids and some plant pigments. The supernatant was collected and evaporated under vacuum at 40 ºC. The residue was dissolved in 0.2 mL methanol/water (20/80, v/v) solution using an ultrasonic bath. The dissolved samples were filtered through 13 mm diameter Millex filters with 0.22 µm pore size nylon membrane (Millipore, Bedford, MA, USA) and placed into opaque microcentrifuge tubes.

Ten µL of filtered extract were injected in a U-HPLC-MS system consisting of an Accela Series U-HPLC (ThermoFisher Scientific, Waltham, MA, USA) coupled to an Exactive mass spectrometer (ThermoFisher Scientific, Waltham, MA, USA) using a heated electrospray ionization (HESI) interface. Mass spectra were obtained using the Xcalibur software version 2.2 (ThermoFisher Scientific, Waltham, MA, USA). Metabolites of interest were identified by extracting the exact mass from the full scan chromatogram obtained in the negative mode and adjusting a mass tolerance of ≤ 1 ppm. The concentrations were semi-quantitatively determined from the extracted peaks using the calibration curves of analog compounds.

Full Paper

Statistical analyses

194

195   The descriptive statistics were calculated by using the StatGraphics Centurion XV software

196   (StatPoint Technologies, Inc. Warrenton, VA, USA) and SPSS 21.0.0 (SPSS Inc., Chicago, IL,

197   USA) programs. Outliers were identified and excluded for posterior analyses as described

198   elsewhere (Alaguero-Cordovilla et al., 2021). We performed multiple testing analyses using the

199   ANOVA F-test or Fisher's least significant difference (LSD) methods (p-value < 0.01,

200   otherwise indicated). Non-parametric tests were used when necessary (i.e. AR emergence and

201   AR number).

RESULTS

Time-course RNA-Seq analysis during wound-induced organ formation in tomato hypocotyl explants

We previously studied wound-induced adventitious root (AR) development in the basal region of Micro-Tom hypocotyl explants (Alaguero-Cordovilla et al., 2021). We observed formative divisions of the cambial cells facing the phloem one day after wounding. AR primordia emerged from specific domains within the basal region of the explants after 3-4 days, and 96.8% of the explants developed between two and four ARs at 8 days (**Figure 1a**) (Alaguero-Cordovilla et al., 2021). Intriguingly, hypocotyl explants obtained by sectioning shoot explants just below the cotyledons developed new functional shoots at their apical end after three weeks (**Figure 1b**, rs). We confirmed the absence of pre-formed shoot apical meristems (SAM) in these explants at T0 that quickly sealed the wound in the apical region (**Figure 1c**, stage 1). We found that homogeneous callus-like tissue formation developed from 4-5 days onwards (**Figure 1c**, stage 2). After 8 days, some regionalization within these calluses occurred and bud outgrowth was obvious (**Figure 1c**, stage 3), which will form new shoot apices afterwards (**Figure 1c**, stage 4).

To reveal the molecular signatures during *de novo* organ formation in tomato, we performed time-course bulk RNA-Seq analysis of apical and basal regions of the hypocotyl explants at 0, 1, 4 and 8 days after wounding (see **Materials and Methods**). We found that 20,831 genes displayed significant transcriptional changes, representing 60% of the tomato genes in ITAG4.0 annotation. About 10 % of transcripts were long non-coding RNA (lncRNA; **Supplemental Figure 1d, e**). We assayed the expression profile of two genes by qRT-PCR (**Supplemental Figure 2a, b**), and these results supported the reliability of our RNA-Seq dataset. Principal component (PC) analysis of expression profiles showed differences in transcript profiling both between apical and basal regions and during the time-course (**Figure 1d**).

Functional enrichment analysis of gene expression profile during wound-induced regeneration

K-means clustering analysis across different time points and hypocotyl regions, was performed using the most variable expressed genes (standard derivation, SD > 0.5), resulting in 4,500 and 4,600 genes from apical and basal regions, respectively (**Supplemental Figure 2c, d**). The optimal cluster number was estimated using the Elbow method implemented in iDEP.91 (Ge et

9

235   al., 2018) (**Supplemental Figure 2e, f**). Three of these clusters displayed the same temporal

236   profile in apical and basal regions, corresponding to genes mostly expressed at T0 (cluster 1),

237   genes expressed at T1 (cluster 2), and genes expressed at T4 and T8 (cluster 3; **Figure 1e, f**).

238   Besides, we found two additional clusters in the apical region, which included genes expressed

239   at T0-T1 (cluster 4) and T1-T4-T8 (cluster 5; **Figure 1e**). Venn diagrams and Gene Ontology

240   (GO) enrichment analysis in clusters 1-3 allowed us to identify either specific (apical or basal)

241   or common GO enrichment subsets (**Supplemental Figure 3** and **Supplemental Table 2**).

242   Genes in cluster 1 might represent the basal transcriptome of young tomato hypocotyls and

243   would reveal tissue-specific differences at T0. Enriched genes shared between apical and basal

244   regions (10.6 %; **Supplemental Figure 3a** and **Supplemental Table 2**) were related to auxin

245   signaling and gibberellin biosynthesis, which are known to contribute to hypocotyl growth

246   (Jiang et al., 2020).

247   Cluster 2 might contain key regulators of *de novo* organ formation as their expression levels

248   transiently increased 24 h after wounding (**Figure 1e, f**). We did not find significant GO

249   enrichment for the common genes in this cluster (**Supplemental Table 2**), which was consistent

250   with our PC analyses and with the divergent developmental patterns at the apical and basal

251   regions after wounding (**Figure 1d**). A GO enriched network for specific genes in the apical

252   region in this cluster was related to nucleosome assembly and chromatin remodeling (**Figure**

253   **2a** and **Supplemental Table 2**). On the other hand, oxidation-reduction processes and GO

254   terms related to hormone biosynthesis and regulation were among the mostly GO enriched

255   terms found in the basal region (**Supplemental Table 2**). Genes in cluster 3 were mostly

256   expressed between T4 and T8 (**Figure 1e, f**). The most-significantly enriched GO terms shared

257   between apical and basal regions were related to cell cycle function (**Figure 2b** and

258   **Supplemental Table 2**). Nevertheless, GO terms related to photosynthesis and *de novo* protein

259   folding were highly enriched in the apical region (**Figure 2c** and **Supplemental Table 2**). On

260   the other hand, highly enriched GO terms in the basal region belonged to cell wall modification

261   and reactive oxygen species (ROS) detoxification (**Supplemental Table 2**). Cluster 4 genes

262   were mostly expressed in the apical region up to 24 h after excision (T1) and were enriched in

263   terms related to cell wall and polysaccharide metabolism (**Figure 1e** and **Supplemental Table**

264   **2**). Cluster 5 genes, which were highly expressed between T1 and T8 in the apical region, were

265   enriched in GO terms related to carbon metabolism-related biosynthetic process (**Figure 1e** and

266   **Supplemental Table 2**).

267   Our GO-enrichment analysis based on K-means gene clustering suggests that both shared
268   and specific biological processes are taking place in the apical and basal regions of the explants
269   during *de novo* organ formation.
270
271   **Differentially expressed genes during wound-induced regeneration**
272   We identified 12,406 deregulated genes (DEG) as regards T0, representing 59.6% of the
273   expressed genes in the RNA-Seq analysis. In the apical region of the explants, we found 8,792
274   DEG (4,658 and 4,265 upregulated and downregulated genes, respectively), whose overlap in
275   different contrasts (**Figure 2d**) allowed us to perform GO term enrichment analysis of specific
276   gene subsets. Within the upregulated genes from T1 to T8 in the apical region, we found
277   enrichment of GO terms associated with serine/glycine metabolism, sterol biosynthesis, and
278   response to oxidative stress (**Supplemental Table 3**). Besides, some genes related to hormone
279   response were downregulated and significantly enriched through the time-course in this region
280   (**Supplemental Table 3**). Downregulated genes at T1 were enriched in GO terms related to
281   photosynthesis (light-dependent reactions) and *de novo* protein folding, while a subset of auxin
282   response genes were upregulated in T1 (**Supplemental Table 3**). Interestingly, we found
283   upregulated genes that were enriched in GO terms related to cell cycle regulation, some of
284   which were shared between T1 and T8 contrasts, while others were specific of T8
285   (**Supplemental Table 3**). Within the downregulated genes at the T4 and T8 contrasts, we found
286   GO terms related to cell wall biogenesis and cell redox homeostasis (**Supplemental Table 3**).
287   Overlapping with leaf primordia formation in this region, some genes annotated as being
288   involved in leaf development were also significantly upregulated at T8 (**Supplemental Table
289   3**).
290   We found 9,085 DEG (4,076 and 5,233 upregulated and downregulated genes, respectively)
291   in the basal region as regards T0 (**Figure 2e**). Within the upregulated genes from T1 to T8
292   (**Supplemental Table 3**), we found enrichment of GO terms associated with ion transport.
293   Some photosynthesis-related genes were downregulated at T1, whereas other genes were also
294   downregulated through the time-course (**Supplemental Table 3**). The GO terms related to
295   protein translation, rRNA modification and RNA processing were enriched at the T1 contrast
296   (**Supplemental Table 3**). For DEG related to cell cycle, a subset of genes involved in cell
297   division was downregulated at T1 while other genes were upregulated at T4 (**Supplemental
298   Table 3**). We also found a contrasting regulation of genes assigned to GO terms related to
299   response to oxidative stress. Indeed, some genes involved in ROS detoxification (mainly
300   encoding peroxidase function) were up-regulated at T4 and T8 contrasts, while genes involved

11

Full Paper

301   in H_2O_2 responses were down-regulated from T1 to T8 (**Supplemental Table 3**). The GO term

302   enrichment for upregulated genes at T4 and T8 highlighted genes involved in cell wall

303   biogenesis, which follows the formation and emergence of AR primordia in the basal region.

304   The biological functions identified by GO term enrichment analyses might contribute to the

305   separate developmental functional processes of tissue reprogramming during *de novo* shoot

306   formation and AR formation in the apical and basal regions of the tomato hypocotyl explants,

307   respectively, and thus deserve further attention.

308

309   **Tissue-specific regulation of photosynthesis during wound-induced organ formation**

310   Our functional GO analysis showed an enrichment in genes related to photosynthesis process

311   during *de novo* organ formation (**Supplemental Table 2** and **3**). Due to the relevance of this

312   metabolic process, we have identified 90 genes in the photosynthesis-related KEGG pathway

313   databasetime-course (**Supplemental Table 4**), 76 of them (84.4%) were deregulated

314   (**Supplemental Figure 4a, b**). Hierarchical clustering analysis of gene expression values

315   highlighted two predominant profiles in the apical region: genes mainly repressed at T1, but

316   that they regain their expression at T4 and T8 (red cluster, **Figure 3a, c),** and genes with an

317   increase in expression from T1 to T8 (purple cluster, **Figure 3a, c**). On the other hand, most

318   photosynthesis-related genes in the basal region showed strong repression in T1 and mild

319   decreased expression at T4 and T8 as regards T0 levels (green cluster, **Figure 3b, c**). These

320   results showed differential gene expression regulation of the photosynthetic machinery in the

321   apical and basal regions after wounding (**Figure 3d-g**). Our DEG analysis uncovered genes

322   involved in regulating the plastoquinone pool (**Supplemental Figure 4a, c**), such as those

323   encoding the NADPH subunits PNSB1 and PNSB4, or those encoding ferredoxins (FD) and

324   the $NADP^+$ reductases LFNR1 and PGR5-like, which were upregulated in the apical region

325   from T1 onwards (**Figure 3d**). In the apical region, most genes encoding core components of

326   PSII were upregulated from T1 onwards (**Figure 3e**). However, most of the genes encoding

327   different PSI proteins were downregulated at T1 in this region, and showed a strong

328   upregulation at T4 and T8 in the apical region (**Figure 3f**). Interestingly, genes encoding

329   antenna proteins of both photosystems (LHCB and LHCA) displayed a severe downregulation

330   of their expression levels in the apical region only at T1 and were downregulated in the basal

331   region from T0 onwards (**Supplemental Figure 4b, d**). In addition to deregulation of genes

332   associated with different components of the photosynthetic machinery in the apical region,

333   regulatory genes encoding the protein kinases ABC1K1 and STN8, as well as the auxiliary PSII

334   core protein PSB33, were also upregulated (**Figure 3g**). Conversely, in the basal region all these

335   genes were significantly downregulated from T1 onwards (**Figure 3g**), suggesting that
336   photosynthesis function might be reduced in the basal region after wounding and during AR
337   formation.

338   To determine the photosynthesis requirement for wound-induced organ formation, we
339   grown hypocotyl explants on different light and photoperiod conditions (**Figure 3h-l**).
340   Hypocotyl explants grown on continuous darkness (0:24 photoperiod) were able to produce
341   ARs in the basal region of the hypocotyl, albeit with severe delay in their emergence (**Figure 3
342   h, i**), but *de novo* organ formation in the apical region of these explants was held at stage 2
343   (**Figure 3 h**). We found that hypocotyl explants incubated for 3 days on standard photoperiod
344   conditions (16 h light and 8 h darkness; 16:8) and then transferred to continuous darkness, were
345   able to overcome stage 2 and did produce new shoots (**Figure 3h**). Taken together, these results
346   indicate that wound-induced *de novo* shoot formation in hypocotyl explants requires the light
347   signal.

348

349   **Tight regulation of ROS homeostasis is required for wound-induced AR formation**
350   Because of photooxidative stress after wounding, light-induced ROS accumulation might occur
351   in hypocotyl explants. Indeed, we found GO term enrichment of genes related to ROS
352   detoxification during the studied time-course (**Supplemental Table 2** and **3)**. To measure ROS
353   production, we visualized H_2O_2 accumulation by DAB staining during wound-induced organ
354   formation (see **Materials and Methods**). At T1, higher DAB staining was found in the apical
355   region of the explants (**Figure 4a**). Interestingly, the DAB precipitate was restricted to the tissue
356   near the wound at T4, both in the apical and the basal region of the explants (**Figure 4a**, T4
357   inset). At T8, DAB staining was much lower and restricted to the most distal cells in the basal
358   region and specific cells within the apical callus (**Figure 4a**, T8 inset). We confirmed DAB-
359   specific staining of H_2O_2 accumulation by catalase incubation (**Figure 4a**, T1 cat).

360   To get additional insight into ROS regulation, we retrieved 135 expressed genes related to
361   ROS homeostasis (**Supplemental Table 5**) that were assigned to different families based on
362   the enzymatic activities of their products (Savelli et al., 2019). A hundred and ten (81.4%) of
363   these genes were DEG (**Figure 4b**). In the apical region, most of the genes encoding ROS
364   scavenging proteins were upregulated as regards T0 (**Supplemental Figure 5a, b**). In addition,
365   five genes encoding membrane-dependent NADPH oxidases of the RBOH family
366   (**Supplemental Figure 5a, b**), involved in stress-induced singlet oxygen production (Sagi et
367   al., 2004; Devireddy et al., 2021), were upregulated both in the apical and the basal region
368   (**Supplemental Figure 5b**). As excessive singlet oxygen might cause increased ROS levels that

13

369   eventually lead to cell death (Gill and Tuteja, 2010), we visualized cell death by trypan blue

370   staining (see **Materials and Methods**; **Figure 4c**). At T1, we found a faint trypan blue staining

371   in the distal end of the apical region and no trypan blue staining in the basal region (**Figure 4c**,

372   T1). At T4, however, trypan blue stained the outer cell layer of the basal region and the most

373   distal cell layer of the apical region of the explants (**Figure 4c**, T4 inset). Similar trypan blue

374   staining was found for distal cells within the apical and the basal regions of the hypocotyl

375   explants **(Figure 4c**, T8), indicating that the extent of ROS was not directly associated

376   with cell death. Genes encoding peroxiredoxins (PRX) and thioredoxins (TRX), ascorbate

377   peroxidases (APX), and catalases (CAT) were differentially regulated between the apical and

378   the basal regions (**Supplemental Figure 5a, b**), which might account for the observed

379   differences in H_2O_2 accumulation upon wounding (**Figure 4a**).

380   We gathered 85 expressed genes encoding class III peroxidases (POX), 81 of which (95.3%)

381   were deregulated largely than other ROS scavenging proteins (**Supplemental Table 5**). We

382   grouped them accordingly to six different expression profiles (**Figure 4d-g**). Forty-one DEG

383   were constitutively upregulated in both the apical region and the basal region during the time-

384   course (e.g. *Prx54*, *Prx68*), with a few of these genes (e.g. *Prx92*, *Prx97*) being downregulated

385   at T1 in the basal region (clusters A and B, respectively; **Figure 4d**). Twenty-nine DEG showed

386   contrasting deregulation in the apical and the basal regions, with 21 of them being upregulated

387   mainly in the basal region (e.g. *Prx100*, *Prx105*, clusters C and D; **Figure 4e**), and eight DEG

388   were upregulated in the apical region only (e.g. *Prx44*, *Prx95*, cluster E; **Figure 4f**). Eleven

389   DEG were mostly downregulated in both tissues as regards T0 (e.g. *Prx20*, *Prx87*, cluster F;

390   **Figure 4g**). Our results indicate differential regulation of POX-encoding genes in the apical

391   and the basal region of the hypocotyl explants during the time-course, which might account for

392   dynamic ROS homeostasis during wound-induced organ formation in tomato hypocotyl

393   explants.

394

395   **Photorespiration is required for wound-induced *de novo* shoot formation**

396   We found 315 expressed genes related to carbon metabolism of which 199 were DEG

397   (**Supplemental Table 6**). Key metabolic pathways, such as glycolysis/gluconeogenesis, carbon

398   fixation through the Calvin-Benson cycle, glycolate/glyoxylate metabolism (i.e.

399   photorespiration) and pentose phosphate pathway, were deregulated in our bulk time-course

400   RNA-Seq (**Supplemental Figure 6a, b**). A subset of these DEG showed contrasting

401   deregulation between apical and basal regions and deserved further attention. Because of the

402   massive downregulation of the photosynthesis machinery at T1 (see above), the energy supply

Full Paper

required for new organ growth might be compromised on the hypocotyl explants. Deregulation of genes encoding key enzymes of the Calvin-Benson cycle for the CO_2 fixation via 3-phosphoglycerate (3-PGA), showed opposite trends in the apical and basal regions as regards T0, which suggest *de novo* establishment of sink-source relationships after wounding in these two regions (**Supplemental Figure 6b**).

Photorespiratory metabolism involves the production of 3-PGA by the oxygenase activity of the RuBisCO enzyme through the glycine and serine pathway at a high metabolic cost (Dellero et al., 2016). Because most genes encoding RuBisCO subunits are highly expressed (**Figure 5a**), and the atmospheric O_2 floods the wounded tissue in the apical region, photorespiration should be active in this tissue. We found that several genes encoding key enzymes of the glycine biosynthesis pathway downstream of 2-phosphoglycolate, such as PGLP1, GLO4, and GGAT, were specifically upregulated as regards T0 in the apical region (**Figure 5a**). In contrast, all these genes were downregulated in the basal region after wounding (**Figure 5a**). Because of this differential regulation, glycine levels, but also H_2O_2 as a sub-product, might increase largely in the apical region. In the next step of the photorespiratory pathway, serine is produced via the glycine decarboxylase complex (GDC) and serine hydroxymethyltransferase (SHM) enzymes (Dellero et al., 2016). *GLP1/2*, which encodes the P-subunit of the GDC, and *SHM1* were upregulated in the apical region as regards T0 (**Figure 5a**). Serine is converted to hydroxypyruvate by the product of *AGT1*, which was also found upregulated in the apical region (**Figure 5a**). Finally, hydroxypyruvate is incorporated into the Calvin-Benson cycle as 3-PGA through the enzyme activities encoded by *HPR* and *GLYK* (**Figure 5a**). As it was found for the previous steps, most of the other genes of the photorespiratory pathway were not deregulated in the basal region after wounding, which clearly indicates that photorespiration is restricted to the apical region during wound-induced organ regeneration in tomato hypocotyl explants. To confirm that the observed gene expression changes contribute to a spatial regulation of photorespiration, we measured the endogenous levels of three pathway metabolic intermediaries (glycolate, glyoxylate and hydroxypyruvate) during *de novo* organ formation by targeted metabolome analysis (see **Materials and Methods**). At wounding time (T0), we did not find significant differences in endogenous levels of the studied intermediaries between apical and basal regions of the explants (**Figure 5b**). However, in all cases we found highly significant differences in the endogenous levels of these intermediaries during the time-course, with the highest levels found in the apical region between T1 and T8 (**Figure 5b**). In agreement with these results, 3-PGA levels were significantly enhanced in the apical region of the explants at T1 and T4, while there were no significant

437 differences at T8 between apical and basal regions (**Figure 5c**). 3-PGA is a key intermediary

438 of both the Calvin-Benson cycle and the glycolysis, which is converted into glyceraldehyde 3-

439 phosphate (G3P) by the phosphoglycerate kinase (PGK) and the glyceraldehyde-phosphate

440 dehydrogenase (GAPA) (**Figure 5a**). We found higher levels of 1,3-bisphosphoglycerate and

441 glyceraldehyde 3-phosphate in the apical region of the explants (**Figure 5c**), which were in

442 agreement with a higher upregulation of the *PGK* and *GAPA* genes in this region (**Figure 5a**).

443 In addition, the genes encoding the enzymes involved in the following steps for regeneration of

444 ribulose 1,5-bisphosphatase in the Calvin-Benson cycle were also differentially regulated in the

445 apical and the basal regions (**Supplemental Figure 6b**).

446 Taken together, these results indicate that the apical region suffers a strong metabolic

447 reprogramming after wounding, being photorespiration a restricted pivotal metabolic pathway

448 that is required for effective *de novo* shoot formation after wounding.

449

450 **Spatial regulation of sugar metabolism during wound-induced organ formation**

451 Due to the presence of sucrose in the regeneration medium, the explants might metabolize

452 sugars through the glycolysis pathway as a direct energy source. Invertases irreversibly

453 hydrolyze sucrose into glucose and fructose (Wan et al., 2018), and are classified accordingly

454 to their subcellular localization in cell wall, cytosolic and vacuolar invertases (CWIN, CIN and

455 VIN; **Supplemental Table 7**) (Proels and Hückelhoven, 2014; Tauzin and Giardina, 2014).

456 Besides, sucrose cleavage is mediated by cytosolic sucrose synthase (SUS) (Stein and Granot,

457 2019). Most genes encoding CIN, VIN and SUS enzymes were downregulated as regards T0

458 in the apical and basal regions (**Figure 6a**). On the other hand, several *CWIN* genes were

459 upregulated in both regions as regards T0 expression (**Figure 6a**). Extracellular glucose and

460 fructose are taken up by plant cells via hexose transporters (Chen et al., 2015; Julius et al., 2017)

461 (**Supplemental Table 7**). We found that several genes encoding SWEET transporters (Manck-

462 Götzenberger and Requena, 2016) were upregulated in apical and basal regions of the explants

463 (e.g. *SWEET10b*, *10c*, *11a*, *12a*, *12b* and *12c*) during the time-course (**Figure 6b**). Additionally,

464 *SUT1*, whose product is involved in apoplastic phloem loading (Slewinski et al., 2009), was

465 specifically upregulated in the apical region during the time-course (**Figure 6b**).

466 Metabolic activation of glucose and fructose involves hexokinase (HK) and fructokinase

467 (FK) enzymes, respectively, which were expressed and were differentially regulated in our

468 RNA-seq (**Figure 6c** and **Supplemental Table 7**). The first downstream regulatory step of the

469 glycolysis pathway involves ATP-dependent phosphofructokinase (PFK) and the

470 pyrophosphate-dependent phosphofructokinase (PFP). We identified eight genes encoding PFK

16

471 enzymes and five genes encoding PFP enzymes (**Supplemental Table 7)**, most of which were

472 upregulated in both regions during the time-course (**Figure 6c**). Several genes encoding

473 pyruvate kinase (PK), another key regulatory enzyme of the glycolytic pathway, were similarly

474 upregulated in the apical and basal regions as regards T0 (**Figure 6c**). These results suggest that

475 sucrose is catabolized to pyruvate both in the apical and the basal regions, while

476 photorespiration provides a surplus of G3P that might also be used for pyruvate production

477 mostly in the apical region (see previous section). Indeed, pyruvate levels slightly increased in

478 the apical region but were not significantly affected in the basal region during the time-course

479 (**Figure 6d**). Importantly, gluconeogenesis might also occur from pyruvate or oxaloacetate, the

480 latter being a direct product of the citrate cycle or the glycolate/glyoxylate cycle. Indeed, the

481 gene encoding the pyruvate, phosphate dikinase (PPDK) was found upregulated in the apical

482 region of the explants during the time-course (**Figure 6c**). Another key regulatory factor in

483 gluconeogenesis is fructose 1,6-bisphosphatase (FBPase), and we found three FBPase-encoding

484 genes that were specifically upregulated in the apical region of the explants from T1 onwards

485 (**Figure 6c**). Taken together, these results confirm the metabolic switch of the apical region

486 from being a sink to becoming a source tissue.

487

488 ***De novo* organ formation in tomato hypocotyl explants depends on sugar availability**

489 Finally, since we identified that both photosynthesis and sucrose metabolism are deregulated in

490 wound-induced organ formation, we assayed the relevance of these two factors during *de novo*

491 organ formation in tomato hypocotyl explants. Dark-grown hypocotyl explants (0:24

492 photoperiod) on sucrose-depleted medium did not produce ARs in the basal region of the

493 explants, and *de novo* organ formation in their apical region was held at stage 1 (**Figure 6e**).

494 On standard photoperiod (16:8) on sucrose-depleted medium, ARs were produced in the basal

495 region of half of the explants, but *de novo* organ formation in the apical region was not observed

496 (**Figure 6e**). To confirm that the observed effect of sucrose on wound-induced organ formation

497 depends on the glycolysis pathway, we grew hypocotyl explants on media supplemented with

498 different sugars during 10 days in the dark (see **Materials and Methods**). When grown in

499 sucrose, fructose or glucose, ARs rapidly emerged and by 5 dae all explants produced at least

500 one AR (**Figure 6f**). Additionally, hypocotyl explants grown on sorbitol-supplemented medium

501 did not produce any AR until the explants were transferred to 16:8 photoperiod at 11 dae

502 (**Figure 6f**). At the end of the experiment (17 dae), we found that hypocotyl explants were able

503 to produce *de novo* shoots (stage 3) with similar proportions (31%-50%) regardless of the sugar

504 that was added (**Figure 6g**). We inhibited glycolysis by incubating hypocotyl explants with 2-

505   deoxyglucose (2-DG) and AR emergence was completely blocked (**Figure 6h, i**). In addition,

506   *de novo* shoot formation was not observed in the apical region of these explants, which were

507   held at stage 1 (**Figure 6i**). These results indicate that exogenous sucrose was essential for

508   effective shoot regeneration in the apical region of the hypocotyl explants, but that was not

509   necessary for AR formation when another energy source is present (e.g.

510   photosynthesis/photorespiration-derived compounds).

DISCUSSION

511

512

513 We have established a new experimental system using Micro-Tom hypocotyl explants to study

514 wound-induced *de novo* shoot formation and AR development without exogenous application

515 of plant hormones (this work; Larriba et al., in preparation). We employed bulk time-course

516 RNA-seq and target metabolite profiling to characterize tissue-specific reprogramming events

517 in tomato hypocotyl explants. Time-course transcriptome analyses of wound-induced *de novo*

518 organ formation have been performed in *Arabidopsis thaliana* (Chen et al., 2016; Efroni et al.,

519 2016; Ikeuchi et al., 2017; Pan et al., 2019). Besides, transcriptome dynamics during tissue-

520 reunion after wounding have been extensively studied in this species (Asahina et al., 2011;

521 Melnyk et al., 2015; Melnyk et al., 2018). These earlier studies have contributed to the

522 understanding of the hormonal crosstalk driving the different tissue reprogramming programs

523 and have allowed the identification of some of the transcriptional regulators involved, but

524 comparative studies with other plant species are limited. Our transcriptome data indicate both

525 tissue-specific differences and divergent developmental patterns at the apical and basal regions

526 of tomato hypocotyl explants after wounding. We also found significant variation in lncRNA

527 expression across the studied tissue regions and through the time-course, suggesting a

528 regulatory role for these non-protein-coding genes in wound-induced organ formation will be

529 addressed in future studies. In our experimental system, AR formation in the basal region of the

530 hypocotyl relies on the activation of resident stem cells due to quick auxin homeostasis

531 regulation after wounding (Alaguero-Cordovilla et al., 2021; Larriba et al., in preparation),

532 while in the apical region, callus formation and metabolic reprogramming precede *de novo*

533 shoot formation (this work).

534 We found differential regulation of photosynthesis-related genes in the apical and basal

535 hypocotyl after wounding. On the one hand, photosynthesis-related genes were strongly

536 downregulated in the basal region during the time-course. On the other hand, most of the

537 photosynthesis-related genes were constitutively upregulated in the apical region after

538 wounding, except those encoding antenna proteins (LHC) and PSI components that were

539 transiently downregulated at T1. As these conditions resembled high-light stress adaptation

540 (Johnson and Wientjes, 2020), the high PSII/PSI ratio in the apical region shortly after

541 wounding might lead to the formation of singlet oxygen and thus cause photo-oxidative

542 damage. Indeed, we observed a local increase of ROS production in the apical region at T1,

543 which was downregulated at the later time point, likely by the enhanced expression of genes

544 encoding FD, PRX and TRX, which participate in fine-tuning chloroplast performance under

545 several stress conditions (Cejudo et al., 2020). In agreement with dynamic regulation of

546 photosynthesis function in the apical region after wounding, the expression of key regulators of

547 light acclimation (ABC1K1, STN8 and PSB33) was specifically upregulated in this tissue. DE-

548 ETIOLATED1 (DET1) is a major repressor of photomorphogenesis that associates with

549 CULLIN4 (CUL4)-based E3 ubiquitin ligases for the degradation of several transcription

550 factors (Lau and Deng, 2012). In mammals, Sox2 is a key transcriptional factor for maintaining

551 pluripotency of stem cells and it has been shown that its protein turnover is regulated by the

552 $CUL4A^{DET1-COP1}$ complex (Cui et al., 2018). Whether a conserved regulatory module,

553 downstream of DET1, is required for wound-induced *de novo* shoot formation in tomato

554 hypocotyl explants needs to be addressed. In summary, our results point to blue light as a novel

555 photoregenerative factor in tomato, although the molecular mechanisms that unleash the

556 regenerative signal requires further investigation.

557 Reprogramming of glucose metabolism in cancer cells even in the presence of atmospheric

558 oxygen (the Warburg effect) is a key event to sustain tumor growth, as high glycolytic flux

559 provides sufficient energy and metabolic intermediates required by the rapidly proliferating

560 cells (Boroughs and Deberardinis, 2015; Yu et al., 2017; Frezza, 2020) .Besides, cancer cells

561 rely on the serine/glycine biosynthetic pathway for the production of one-carbon (C_1)

562 metabolites required for tumorous growth (Amelio et al., 2014; Li and Ye, 2020). We

563 demonstrated that wound-induced organ formation in tomato hypocotyl explants, both ARs and

564 *de novo* shoot formation, was dependent on the sugar supply. Several sugar transporters of the

565 SWEET family and CWIN were constitutively upregulated in both the apical and the basal

566 regions of the hypocotyl after wounding. Mirroring what has been found during zebrafish heart

567 regeneration (Honkoop et al., 2019), blocking glycolysis with 2-deoxyglucose impaired the

568 ability of cells near the wound to produce new organs. These results suggest that glycolysis-

569 derived energy (ATP) drives cell proliferation in tomato hypocotyl explants required for

570 wound-induced organ formation, and thus these tissues were rapidly reprogrammed as sink

571 tissues as regards sugar assimilation.

572 We found specific upregulation of the photorespiratory pathway in the apical region of

573 tomato hypocotyl explants after wounding and during *de novo* shoot formation.

574 Photorespiration recycles toxic 2-phosphoglycolate into 3-PGA, which can enter the Calvin–

575 Benson cycle, and it is a key metabolite driving C_1 metabolism in plants (Eisenhut et al., 2019).

576 We hypothesized that initial callus growth in the apical region of the hypocotyl relies on

577 photorespiration-produced 3-PGA, which could be used as a substrate for gluconeogenesis too.

20

578   Indeed, we found differential upregulation of key genes of gluconeogenesis (*PPDK*, *FBPase*)

579   that correlated with increased levels of the intermediates of these two pathways (glyoxylate,

580   hydroxypyruvate, 3-PGA, G3P) in the apical region of the explants. By local inhibition of

581   photorespiration in the apical region, we provide additional evidence of a functional role of this

582   pathway to sustain proliferation and callus formation, which preceded and was required for

583   wound-induced shoot initiation. Our results highlight the key role of photorespiration,

584   considered as an energetically inefficient pathway, to trigger wound-induced *de novo* shoot

585   formation, in light with its proposed role to overcome abiotic stresses (Sunil et al. 2019).

586   Taken together, our results indicate that wounding induced a broad metabolic

587   reprogramming of some cells in the apical region of the hypocotyl (photosynthesis reactivation,

588   photorespiration induction, and high glycolysis), providing energy and structural elements

589   required for rapid proliferation during initial callus growth and that are essential for fate

590   reprogramming required for *de novo* shoot formation.

591   We found striking patterns of ROS accumulation in the apical and basal region of the

592   hypocotyl during the studied time-course, which was not directly correlated with the extent of

593   cell death (this work), and hence might have a signaling role in *de novo* organ formation. ROS

594   accumulation in the basal region of the hypocotyl explants at T4 and T8 might be related to AR

595   emergence (Mhimdi and Pérez-Pérez, 2020). Indeed, during primary root (PR) and lateral root

596   (LR) development in *Arabidopsis thaliana*, ROS distribution (which is regulated by specific

597   POX enzymes) is required for transition between proliferating and differentiating cells in the

598   meristem (Tsukagoshi et al., 2010; Fernández-Marcos et al., 2017). POX display different

599   functions besides their direct role in wounding response (Minibayeva et al., 2015; Shigeto and

600   Tsutsumi, 2016). Indeed, some of the POX-encoding genes were strongly deregulated in our

601   RNA-seq. Interestingly, a subset of class III POX genes was targeted by LATERAL ORGAN

602   BOUNDARIES DOMAIN29 (LBD29) in Arabidopsis (Xu et al., 2018), a master regulator of

603   auxin-induced callus formation (Fan et al., 2012). Moreover, the LBD29-regulated biological

604   responses largely resemble those of hypoxia treatment, which has been long considered as a

605   crucial factor in determining cell fate in mammals (Xu et al., 2018). We found upregulated in

606   the apical region several *POX* genes (*Prx05*, *Prx11*, *Prx25*, *Prx26*, *Prx38* and *Prx68*) that were

607   structurally related to the LBD targets described above, suggesting that some LBD29-gene

608   regulatory networks might be conserved in tomato. Natural variation in hormone-induced shoot

609   regeneration among Arabidopsis accessions was dependent on the expression of a TRX-

610   encoding gene that directly modulates ROS homeostasis (Zhang et al., 2018). Despite

611   differences in wound response between animals and plants, ROS is a common signal in both

Full Paper

612   systems (Suzuki and Mittler, 2012). In cancer cells, the increase of ROS stabilizes the Hypoxia-

613   Inducible Factor-1α (HIF1α) that upregulates glucose catabolism and allows tumor progression

614   (Nagao et al., 2019). Furthermore, iPSC reprogramming is enhanced under hypoxic conditions

615   through ROS-mediated activation of HIF1α (Hawkins et al., 2016). Importantly, transient ROS

616   signaling during early reprogramming demethylates the promoter of a gene encoding the

617   homeobox protein NANOG required for stem cell pluripotency (Ying et al., 2016). A similar

618   hypoxia-mediated mechanism may be present in plants, but operating on the negative regulators

619   of the ERF-VII transcription factors instead (Pucciariello and Perata, 2021). However, a direct

620   link between ROS production, metabolic reprogramming, and wound-induced organ

621   regeneration in tomato hypocotyl explants awaits experimental confirmation.

22

REFERENCES

Alaguero-Cordovilla A, Gran-Gómez FJ, Jadczak P, Mhimdi M, Ibáñez S, Bres C, Just D, Rothan C, Pérez-Pérez JM (2020) A quick protocol for the identification and characterization of early growth mutants in tomato. Plant Sci **301**: 110673

Alaguero-Cordovilla A, Sánchez-García AB, Ibáñez S, Albacete A, Cano A, Acosta M, Pérez-Pérez JM (2021) An auxin-mediated regulatory framework for wound-induced adventitious root formation in tomato shoot explants. Plant Cell Environ pce.14001

Albacete A, Ghanem ME, Martínez-Andújar C, Acosta M, Sánchez-Bravo J, Martínez V, Lutts S, Dodd IC, Pérez-Alfocea F (2008) Hormonal changes in relation to biomass partitioning and shoot growth impairment in salinized tomato (Solanum lycopersicum L.) plants. J Exp Bot **59**: 4119–4131

Amelio I, Cutruzzolá F, Antonov A, Agostini M, Melino G (2014) Serine and glycine metabolism in cancer. Trends Biochem Sci **39**: 191–198

Aryee MJ, Gutiérrez-Pabello JA, Kramnik I, Maiti T, Quackenbush J (2009) An improved empirical bayes approach to estimating differential gene expression in microarray time-course data: BETR (Bayesian Estimation of Temporal Regulation). BMC Bioinformatics **10**: 409

Asahina M, Azuma K, Pitaksaringkarn W, Yamazaki T, Mitsuda N, Ohme-Takagi M, Yamaguchi S, Kamiya Y, Okada K, Nishimura T, et al (2011) Spatially selective hormonal control of RAP2.6L and ANAC071 transcription factors involved in tissue reunion in Arabidopsis. Proc Natl Acad Sci U S A **108**: 16128–16132

Bolger A, Scossa F, Bolger ME, Lanz C, Maumus F, Tohge T, Quesneville H, Alseekh S, Sørensen I, Lichtenstein G, et al (2014) The genome of the stress-tolerant wild tomato species Solanum pennellii. Nat Genet **46**: 1034–1038

Bolser DM, Staines DM, Perry E, Kersey PJ (2017) Ensembl plants: Integrating tools for visualizing, mining, and analyzing plant genomic data. Methods Mol. Biol. Humana Press Inc., pp 1–31

Boroughs LK, Deberardinis RJ (2015) Metabolic pathways promoting cancer cell survival and growth. Nat Cell Biol **17**: 351–359

Cejudo FJ, González M-C, Pérez-Ruiz JM (2020) Redox regulation of chloroplast metabolism. Plant Physiol. doi: 10.1093/plphys/kiaa062

Chen L-Q, Cheung LS, Feng L, Tanner W, Frommer WB (2015) Transport of Sugars. Annu Rev Biochem **84**: 865–894

655 **Chen X, Cheng J, Chen L, Zhang G, Huang H, Zhang Y, Xu L** (2016) Auxin-Independent
656   NAC pathway acts in response to explant-specific wounding and promotes root tip
657   emergence during de novo root organogenesis in arabidopsis. Plant Physiol **170**: 2136–
658   2145

659 **Cliff TS, Dalton S** (2017) Metabolic switching and cell fate decisions: implications for
660   pluripotency, reprogramming and development. Curr Opin Genet Dev **46**: 44–49

661 **Cui CP, Zhang Y, Wang C, Yuan F, Li H, Yao Y, Chen Y, Li C, Wei W, Liu CH, et al**
662   (2018) Dynamic ubiquitylation of Sox2 regulates proteostasis and governs neural
663   progenitor cell differentiation. Nat Commun. doi: 10.1038/s41467-018-07025-z

664 **Dahan-Meir T, Filler-Hayut S, Melamed-Bessudo C, Bocobza S, Czosnek H, Aharoni A,**
665   **Levy AA** (2018) Efficient in planta gene targeting in tomato using geminiviral replicons
666   and the CRISPR/Cas9 system. Plant J **95**: 5–16

667 **Dellero Y, Jossier M, Schmitz J, Maurino VG, Hodges M** (2016) Photorespiratory
668   glycolate–glyoxylate metabolism. J Exp Bot **67**: 3041–3052

669 **Devireddy AR, Zandalinas SI, Fichman Y, Mittler R** (2021) Integration of reactive oxygen
670   species and hormone signaling during abiotic stress. Plant J **105**: 459–476

671 **Dobin A, Davis CA, Schlesinger F, Drenkow J, Zaleski C, Jha S, Batut P, Chaisson M,**
672   **Gingeras TR** (2013) STAR: Ultrafast universal RNA-seq aligner. Bioinformatics **29**:
673   15–21

674 **Efroni I, Mello A, Nawy T, Ip PL, Rahni R, Delrose N, Powers A, Satija R, Birnbaum**
675   **KD** (2016) Root Regeneration Triggers an Embryo-like Sequence Guided by Hormonal
676   Interactions. Cell **165**: 1721–1733

677 **Eisenhut M, Roell M, Weber APM** (2019) Mechanistic understanding of photorespiration
678   paves the way to a new green revolution. New Phytol **223**: 1762–1769

679 **Fan M, Xu C, Xu K, Hu Y** (2012) LATERAL ORGAN BOUNDARIES DOMAIN
680   transcription factors direct callus formation in Arabidopsis regeneration. Cell Res **22**:
681   1169–1180

682 **Feller C, Bleiholder H, Buhr L, Hack H, Hess M, Klose R, Meier U, Stauss R, Van den**
683   **Boom T, Weber E** (1995) Phänologische entwicklungsstadien von gemüsepflanzen: II.
684   Fruchtgemüse und hülsenfrüchte. Nachrichtenbl Deut Pflanzenschutzd **47**: 217–232

685 **Fernández-Marcos M, Desvoyes B, Manzano C, Liberman LM, Benfey PN, del Pozo JC,**
686   **Gutierrez C** (2017) Control of Arabidopsis lateral root primordium boundaries by
687   MYB36. New Phytol **213**: 105–112

688 **Frezza C** (2020) Metabolism and cancer: the future is now. Br J Cancer **122**: 133–135

689 **Ge SX, Jung D, Yao R** (2020) ShinyGO: a graphical gene-set enrichment tool for animals
690   and plants. Bioinformatics **36**: 2628–2629

691 **Ge SX, Son EW, Yao R** (2018) iDEP: An integrated web application for differential
692   expression and pathway analysis of RNA-Seq data. BMC Bioinformatics **19**: 1–24

693 **Gill SS, Tuteja N** (2010) Reactive oxygen species and antioxidant machinery in abiotic stress
694   tolerance in crop plants. Plant Physiol Biochem **48**: 909–930

695 **Hawkins KE, Joy S, Delhove JMKM, Kotiadis VN, Fernandez E, Fitzpatrick LM,**
696   **Whiteford JR, King PJ, Bolanos JP, Duchen MR, et al** (2016) NRF2 Orchestrates the
697   Metabolic Shift during Induced Pluripotent Stem Cell Reprogramming. Cell Rep **14**:
698   1883–1891

699 **Honkoop H, de Bakker DEM, Aharonov A, Kruse F, Shakked A, Nguyen PD, de Heus**
700   **C, Garric L, J Muraro M, Shoffner A, et al** (2019) Single-cell analysis uncovers that
701   metabolic reprogramming by ErbB2 signaling is essential for cardiomyocyte
702   proliferation in the regenerating heart. Elife. doi: 10.7554/eLife.50163

703 **Hosmani PS, Flores-Gonzalez M, van de Geest H, Maumus F, Bakker L V., Schijlen E,**
704   **van Haarst J, Cordewener J, Sanchez-Perez G, Peters S, et al** (2019) An improved de
705   novo assembly and annotation of the tomato reference genome using single-molecule
706   sequencing, Hi-C proximity ligation and optical maps. bioRxiv 767764

707 **Ibáñez S, Carneros E, Testillano PS, Pérez-Pérez JM** (2020) Advances in plant
708   regeneration: Shake, rattle and roll. Plants **9**: 1–19

709 **Ikeuchi M, Favero DS, Sakamoto Y, Iwase A, Coleman D, Rymen B, Sugimoto K** (2019)
710   Molecular Mechanisms of Plant Regeneration. Annu Rev Plant Biol **70**: 377–406

711 **Ikeuchi M, Iwase A, Rymen B, Lambolez A, Kojima M, Takebayashi Y, Heyman J,**
712   **Watanabe S, Seo M, De Veylder L, et al** (2017) Wounding triggers callus formation
713   via dynamic hormonal and transcriptional changes. Plant Physiol **175**: 1158–1174

714 **Ikeuchi M, Ogawa Y, Iwase A, Sugimoto K** (2016) Plant regeneration: Cellular origins and
715   molecular mechanisms. Dev **143**: 1442–1451

716 **Ikeuchi M, Rymen B, Sugimoto K** (2020) How do plants transduce wound signals to induce
717   tissue repair and organ regeneration? Curr Opin Plant Biol **57**: 72–77

718 **Iwase A, Mita K, Favero DS, Mitsuda N, Sasaki R, Kobayshi M, Takebayashi Y, Kojima**
719   **M, Kusano M, Oikawa A, et al** (2018) WIND1 induces dynamic metabolomic
720   reprogramming during regeneration in Brassica napus. Dev Biol **442**: 40–52

721 **Jiang H, Shui Z, Xu L, Yang Y, Li Y, Yuan X, Shang J, Asghar MA, Wu X, Yu L, et al**
722   (2020) Gibberellins modulate shade-induced soybean hypocotyl elongation downstream

25

723   of the mutual promotion of auxin and brassinosteroids. Plant Physiol Biochem **150**: 209–
724   221

725 **Johnson MP, Wientjes E** (2020) The relevance of dynamic thylakoid organisation to
726   photosynthetic regulation. Biochim Biophys Acta - Bioenerg **1861**: 148039

727 **Julius BT, Leach KA, Tran TM, Mertz RA, Braun DM** (2017) Sugar transporters in
728   plants: New insights and discoveries. Plant Cell Physiol **58**: 1442–1460

729 **Kanehisa M, Furumichi M, Sato Y, Ishiguro-Watanabe M, Tanabe M** (2021) KEGG:
730   Integrating viruses and cellular organisms. Nucleic Acids Res **49**: D545–D551

731 **Lau OS, Deng XW** (2012) The photomorphogenic repressors COP1 and DET1: 20 years
732   later. Trends Plant Sci **17**: 584–593

733 **Li AM, Ye J** (2020) Reprogramming of serine, glycine and one-carbon metabolism in cancer.
734   Biochim Biophys Acta - Mol Basis Dis. doi: 10.1016/j.bbadis.2020.165841

735 **Liao Y, Smyth GK, Shi W** (2019) The R package Rsubread is easier, faster, cheaper and
736   better for alignment and quantification of RNA sequencing reads. Nucleic Acids Res **47**:
737   e47–e47

738 **Manck-Götzenberger J, Requena N** (2016) Arbuscular mycorrhiza Symbiosis Induces a
739   Major Transcriptional Reprogramming of the Potato SWEET Sugar Transporter Family.
740   Front Plant Sci **7**: 487

741 **Mathew MM, Prasad K** (2021) Model systems for regeneration: *Arabidopsis*. Development
742   **148**: dev195347

743 **Melnyk CW, Gabel A, Hardcastle TJ, Robinson S, Miyashima S, Grosse I, Meyerowitz**
744   **EM** (2018) Transcriptome dynamics at Arabidopsis graft junctions reveal an intertissue
745   recognition mechanism that activates vascular regeneration. Proc Natl Acad Sci U S A
746   **115**: E2447–E2456

747 **Melnyk CW, Schuster C, Leyser O, Meyerowitz EM** (2015) A developmental framework
748   for graft formation and vascular reconnection in arabidopsis thaliana. Curr Biol **25**:
749   1306–1318

750 **Mhimdi M, Pérez-Pérez JM** (2020) Understanding of Adventitious Root Formation: What
751   Can We Learn From Comparative Genetics? Front Plant Sci **11**: 1541

752 **Minibayeva F, Beckett RP, Kranner I** (2015) Roles of apoplastic peroxidases in plant
753   response to wounding. Phytochemistry **112**: 122–129

754 **Nagao A, Kobayashi M, Koyasu S, Chow CCT, Harada H** (2019) HIF-1-dependent
755   reprogramming of glucose metabolic pathway of cancer cells and its therapeutic
756   significance. Int J Mol Sci. doi: 10.3390/ijms20020238

Full Paper

757   **Okabe Y, Ariizumi T, Ezura H** (2013) Updating the Micro-Tom TILLING platform. Breed

758   Sci **63**: 42–48

759   **Pan J, Zhao F, Zhang G, Pan Y, Sun L, Bao N, Qin P, Chen L, Yu J, Zhang Y, et al**

760   (2019) Control of de novo root regeneration efficiency by developmental status of

761   Arabidopsis leaf explants. J Genet Genomics **46**: 133–140

762   **Panopoulos AD, Yanes O, Ruiz S, Kida YS, Diep D, Tautenhahn R, Herrerías A,**

763   **Batchelder EM, Plongthongkum N, Lutz M, et al** (2012) The metabolome of induced

764   pluripotent stem cells reveals metabolic changes occurring in somatic cell

765   reprogramming. Cell Res **22**: 168–177

766   **Proels RK, Hückelhoven R** (2014) Cell-wall invertases, key enzymes in the modulation of

767   plant metabolism during defence responses. Mol Plant Pathol **15**: 858–864

768   **Pucciariello C, Perata P** (2021) The Oxidative Paradox in Low Oxygen Stress in Plants.

769   Antioxidants **10**: 332

770   **Sagi M, Davydov O, Orazova S, Yesbergenova Z, Ophir R, Stratmann JW, Fluhr R**

771   (2004) Plant respiratory burst oxidase homologs impinge on wound responsiveness and

772   development in Lycopersicon esculentum. Plant Cell **16**: 616–628

773   **Savelli B, Li Q, Webber M, Jemmat AM, Robitaille A, Zamocky M, Mathé C, Dunand C**

774   (2019) RedoxiBase: A database for ROS homeostasis regulated proteins. Redox Biol **26**:

775   101247

776   **Shigeto J, Tsutsumi Y** (2016) Diverse functions and reactions of class III peroxidases. New

777   Phytol **209**: 1395–1402

778   **Shikata M, Ezura H** (2016) Micro-tom tomato as an alternative plant model system: Mutant

779   collection and efficient transformation. Methods Mol. Biol. Humana Press Inc., pp 47–55

780   **Slewinski TL, Meeley R, Braun DM** (2009) Sucrose transporter1 functions in phloem

781   loading in maize leaves. J Exp Bot **60**: 881–892

782   **Stein O, Granot D** (2019) An overview of sucrose synthases in plants. Front Plant Sci **10**: 95

783   **Suzuki N, Mittler R** (2012) Reactive oxygen species-dependent wound responses in animals

784   and plants. Free Radic Biol Med **53**: 2269–2276

785   **Takahashi K, Yamanaka S** (2006) Induction of Pluripotent Stem Cells from Mouse

786   Embryonic and Adult Fibroblast Cultures by Defined Factors. Cell **126**: 663–676

787   **Tauzin AS, Giardina T** (2014) Sucrose and invertases, a part of the plant defense response to

788   the biotic stresses. Front Plant Sci **5**: 293

789   **Tsukagoshi H, Busch W, Benfey PN** (2010) Transcriptional regulation of ROS controls

790   transition from proliferation to differentiation in the root. Cell **143**: 606–616

Full Paper

791   **Wan H, Wu L, Yang Y, Zhou G, Ruan YL** (2018) Evolution of Sucrose Metabolism: The

792   Dichotomy of Invertases and Beyond. Trends Plant Sci **23**: 163–177

793   **Xu C, Cao H, Xu E, Zhang S, Hu Y** (2018) Genome-Wide Identification of Arabidopsis

794   LBD29 Target Genes Reveals the Molecular Events behind Auxin-Induced Cell

795   Reprogramming during Callus Formation. Plant Cell Physiol **59**: 749–760

796   **Ying Z, Chen K, Zheng L, Wu Y, Li L, Wang R, Long Q, Yang L, Guo J, Yao D, et al**

797   (2016) Transient Activation of Mitoflashes Modulates Nanog at the Early Phase of

798   Somatic Cell Reprogramming. Cell Metab **23**: 220–226

799   **Yu L, Chen X, Sun X, Wang L, Chen S** (2017) The glycolytic switch in tumors: How many

800   players are involved? J Cancer **8**: 3430–3440

801   **Zhang H, Zhang TT, Liu H, Shi DY, Wang M, Bie XM, Li XG, Zhang XS** (2018)

802   Thioredoxin-Mediated ROS Homeostasis Explains Natural Variation in Plant

803   Regeneration. Plant Physiol **176**: 2231–2250

28

Full Paper

ACKNOWLEDGEMENTS

806

ADDITIONAL INFORMATION

Competing interests

809   The authors declare that they have no competing interests.

810

Funding

816

### Authors' contributions

818   JMPP designed the research. EL, ABSG, CMA and AA performed the research and analyzed the data. JMPP wrote the manuscript with the assistance of EL. All authors read and approved the final manuscript.

821

Data Availability Statement

823   Raw sequence files and read count files are publicly available in the NCBI's BioProject repository upon publication. Gene functional annotation is available in the supplementary material of this article. All other data that support the findings of this study are available from the corresponding author upon reasonable request.

29

Full Paper

Figure 1

827

828
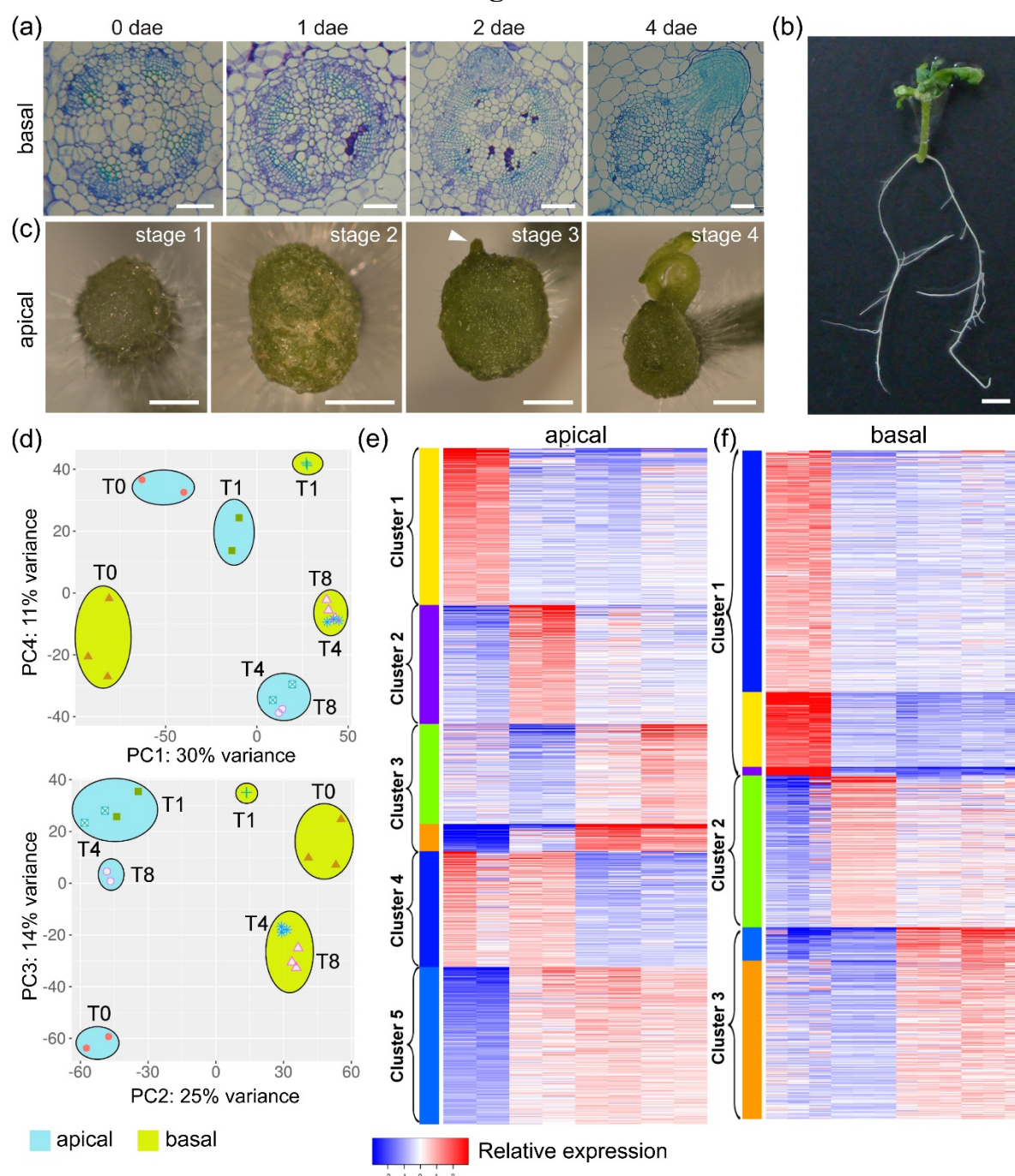
829   **Figure 1**. **Wound-induced organ formation in tomato hypocotyl explants**. (a) Adventitious
830   root (AR) development in the basal region of the hypocotyl explants. (b) Whole plant
831   regeneration from hypocotyl and stem node explants at 21 dae; rs: regenerated shoot. (c)
832   Developmental stages during *de novo* shoot formation in the apical region of the hypocotyl.
833   Scale bars: 100 µm (a), 1 mm (b) and 4 mm (c). (d) Principal component (PC) analysis of the
834   RNA-Seq results. (e, f) K-means clustering of time-course RNA-Seq results from apical (e) and
835   basal (f) regions of the hypocotyl. Predicted clusters are colored and grouped accordingly to its
836   temporal expression profile.

837

30

838

Figure 2

839
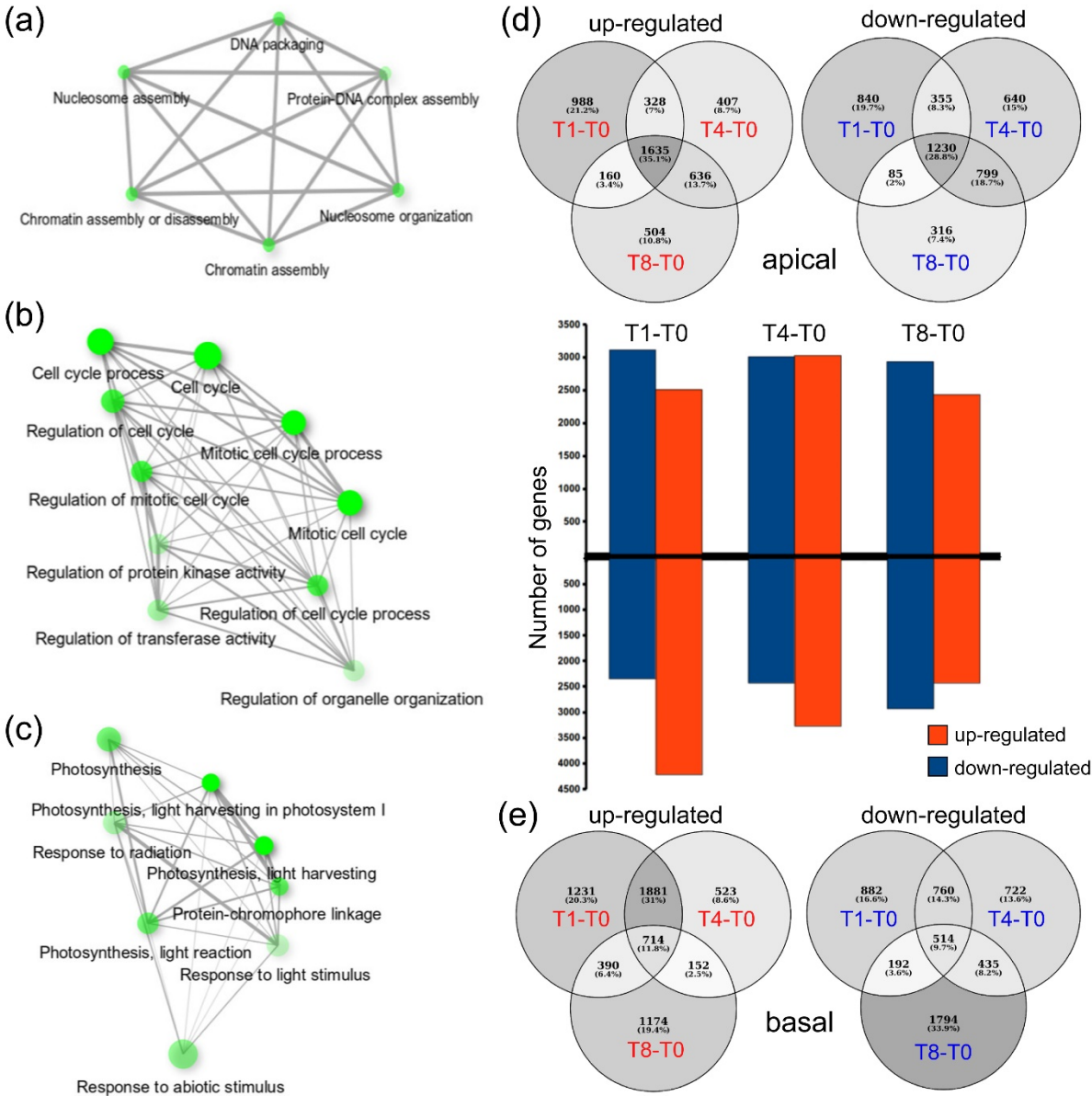
840 **Figure 2. Functional enrichment and DEG analysis during wound-induced regeneration**.
841 (a-c) Examples of GO term-enriched networks of the upregulated genes in the apical region at
842 T1 (a), of the upregulated genes at T4-T8 shared between apical and basal regions (b), and of
843 specific upregulated genes in the apical region at T4-T8 (c). (d, e) Venn diagrams of upregulated
844 and downregulated DEGs, from apical (d) and basal (e) regions of the hypocotyl as regards T0.

Full Paper
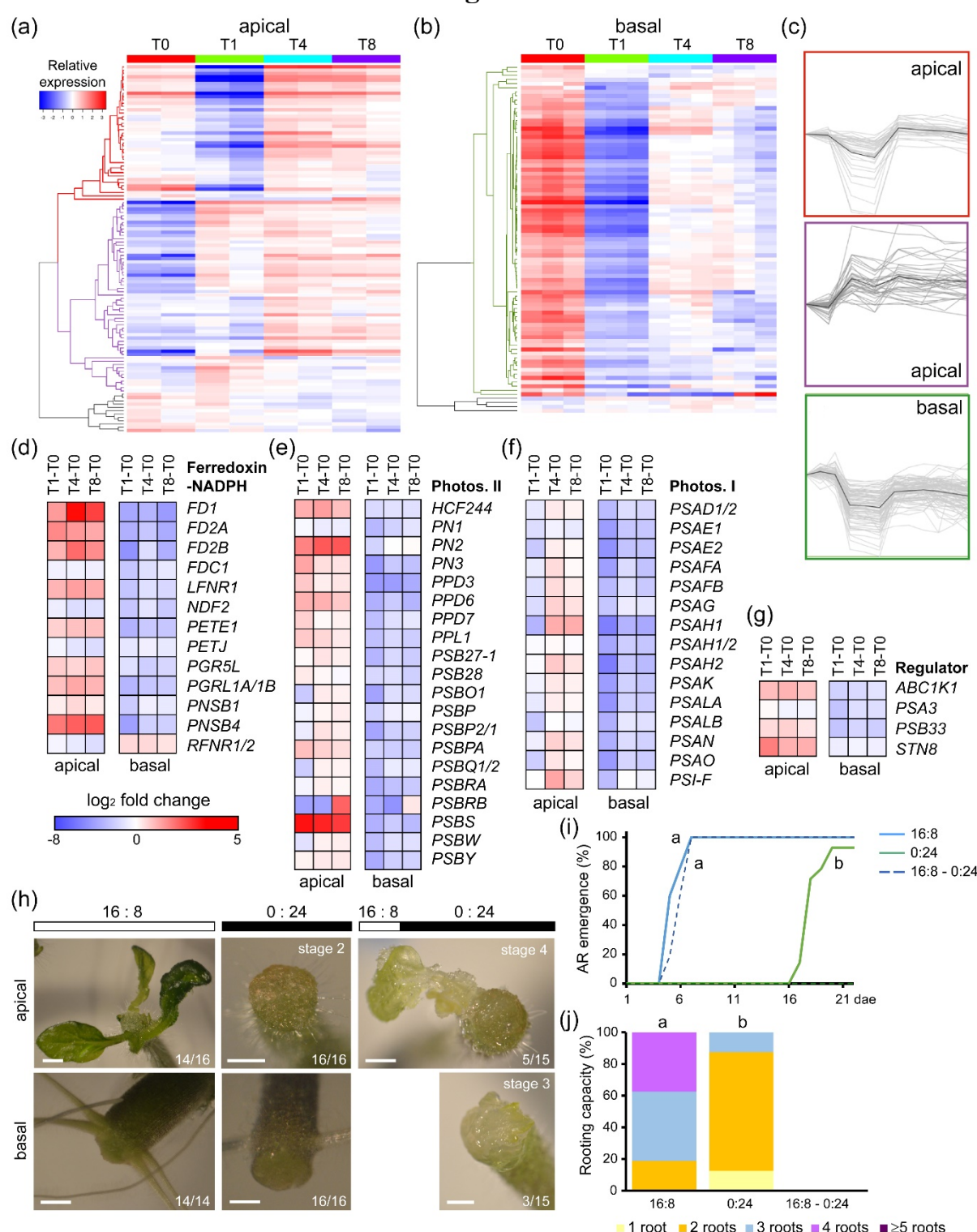
Figure 3

Figure 3. Regulation of photosynthesis-related genes during wound-induced organ formation. (a, b) Hierarchical clustering of the time-course expression of photosynthesis genes in the apical (a) and basal (b) regions of the hypocotyl explants. (c) Expression profiles of some of the gene clusters identified. (d-g) DEG involved in know photosynthesis subcomplexes, such as (d) ferredoxin:NAPDH reductase, (e) photosystem II or (f) photosystem I, and in (g) key regulators. (h) Representative images of wound-induced organ formation in the apical and basal region of the hypocotyl explants on different photoperiod conditions: 21-days standard

854   photoperiod (16 h light and 8 h darkness; 16:8), 21-days darkness (0 h light and 24 h darkness;
855   0:24), and 3 days on 16:8 photoperiod followed by 18 days on 0:24 photoperiod. Gene
856   annotations (d-g) are found in Supplemental Table 4. Scale bars: 1 mm.

857

Figure 4
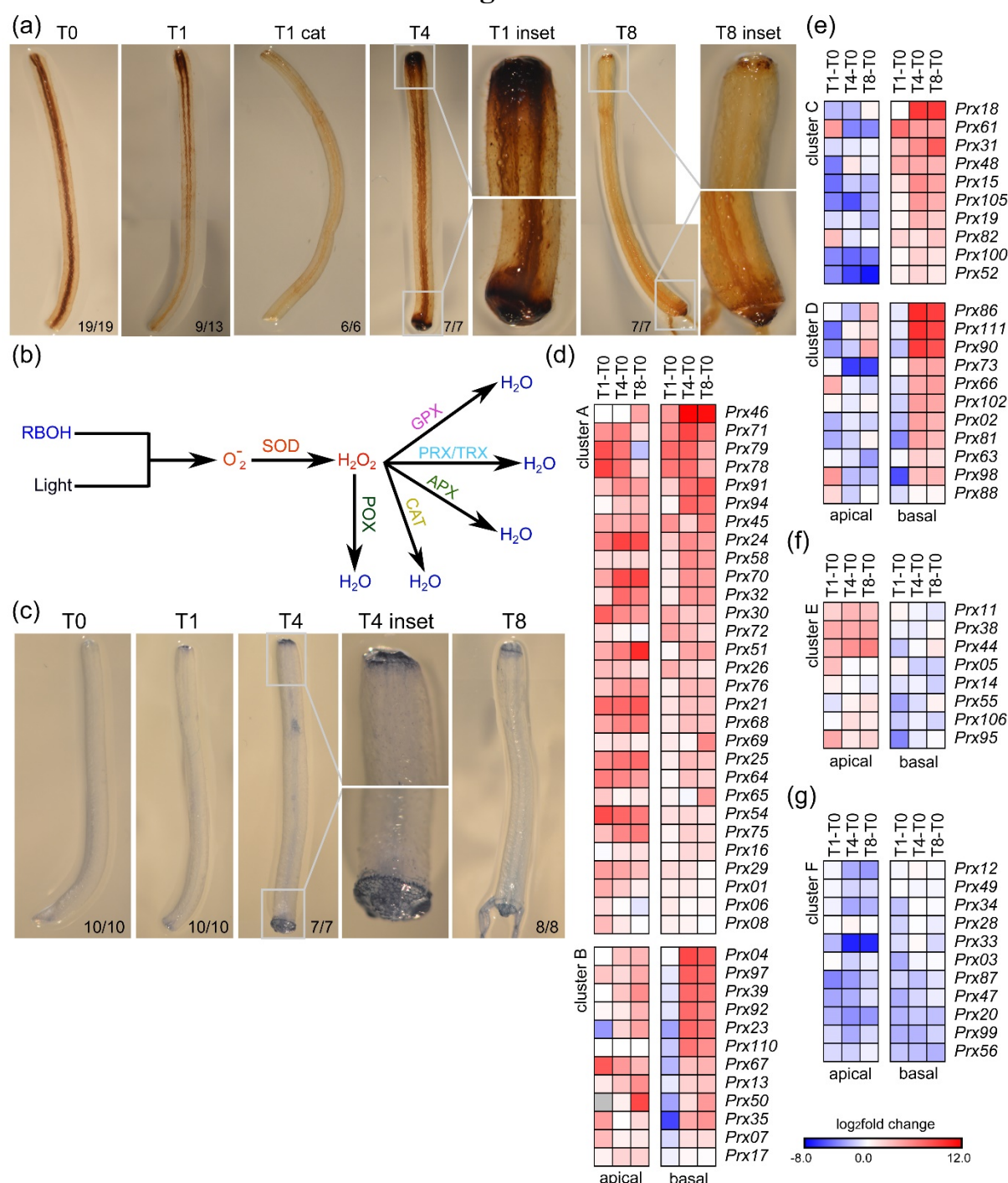
858
859 **Figure 4. Reactive oxygen species (ROS) regulation during wound-induced organ**
860 **formation**. (a) H_2O_2 accumulation visualized by DAB staining in the hypocotyl explants during
861 the studied time-course. (b) Proposed pathways of ROS production and detoxification with key
862 enzymatic activities indicated: RBOH, NADPH oxidase/respiratory burst oxidase homolog;
863 SOD, superoxide dismutase; POX, peroxidase; GPX, glutathione peroxidase; PRX/TRX,
864 peroxiredoxins/thioredoxins; APX, ascorbate peroxidases; CAT, catalases. (c) Localized cell
865 death in the hypocotyl explants during the studied time-course visualized by trypan blue
866 staining. (d-f) Hierarchical clustering of DEG encoding class III peroxidases. Gene annotations
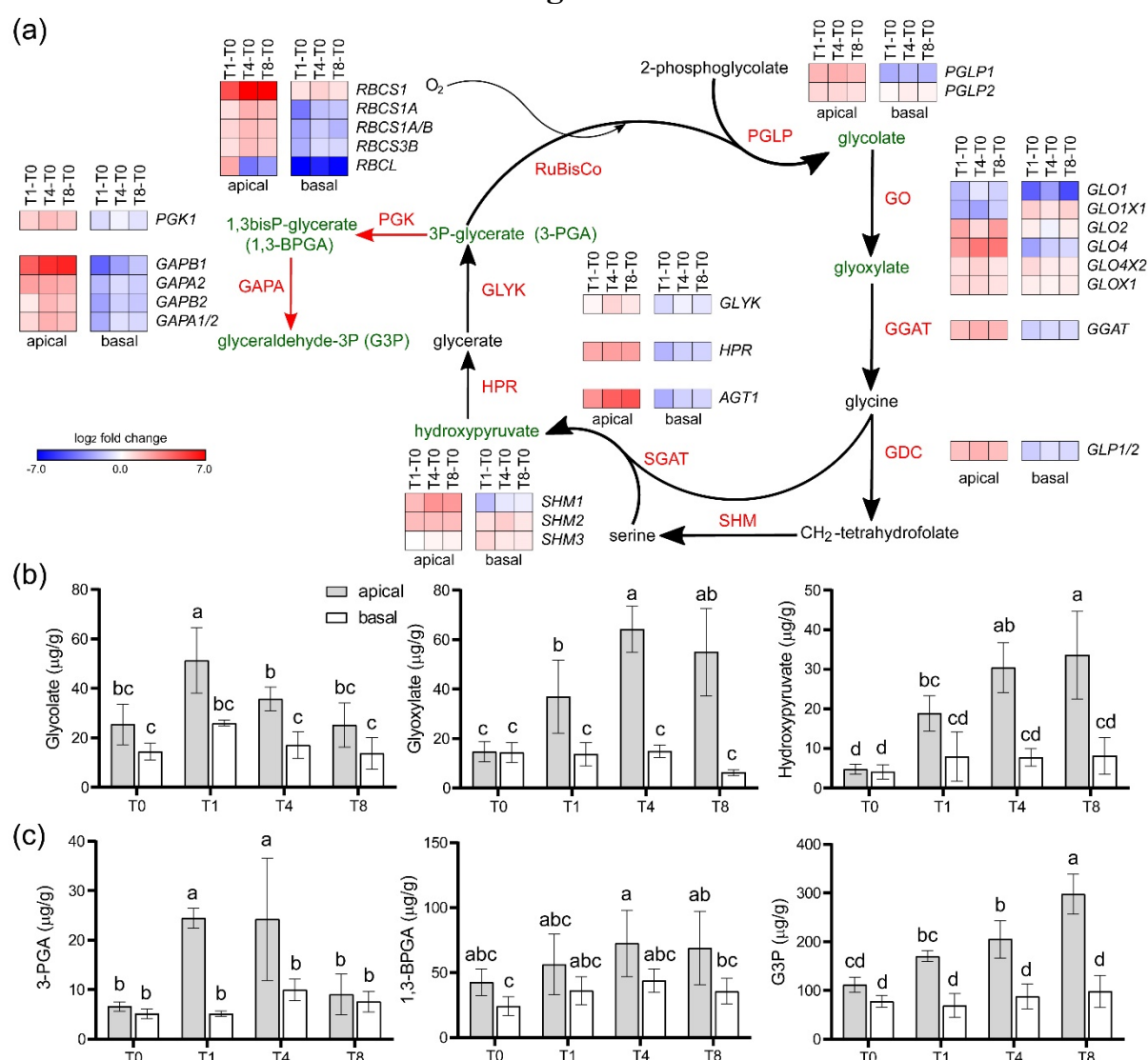867 are found in Supplemental Table 5. Scale bars (a, c): 4 mm.

Full Paper

868

Figure 5

869
870 **Figure 5**. **Photorespiration pathway activation during wound-induced organ formation**.
871 (a) DEG involved in photorespiration. Genes encoding the enzymatic activities of the different
872 steps in the pathway are shown: PGLP, phosphoglycolate phosphatase; GO, glycolate oxidase;
873 GGAT, glutamate-glyoxylate aminotransferase; GDC, glycine decarboxylase complex; SHM,
874 serine hydroxymethyltransferase; SGAT, serine-glyoxylate aminotransferase; HPR,
875 hydroxypyruvate reductase; GLYK, glycerate kinase. Two enzymes of the Calvin-Benson cycle
876 are also included: PGK, phosphoglycerate kinase; GAPA, glyceraldehyde-phosphate
877 dehydrogenase. (b, c) Endogenous levels of several metabolites of the photorespiration pathway
878 in the apical and basal region of the hypocotyl explants during the studied time-course.
879 Different letters indicate significant differences (p-value<0.01) between the assayed conditions.
880 Gene annotations (a) are found in Supplemental Table 6.

Full Paper
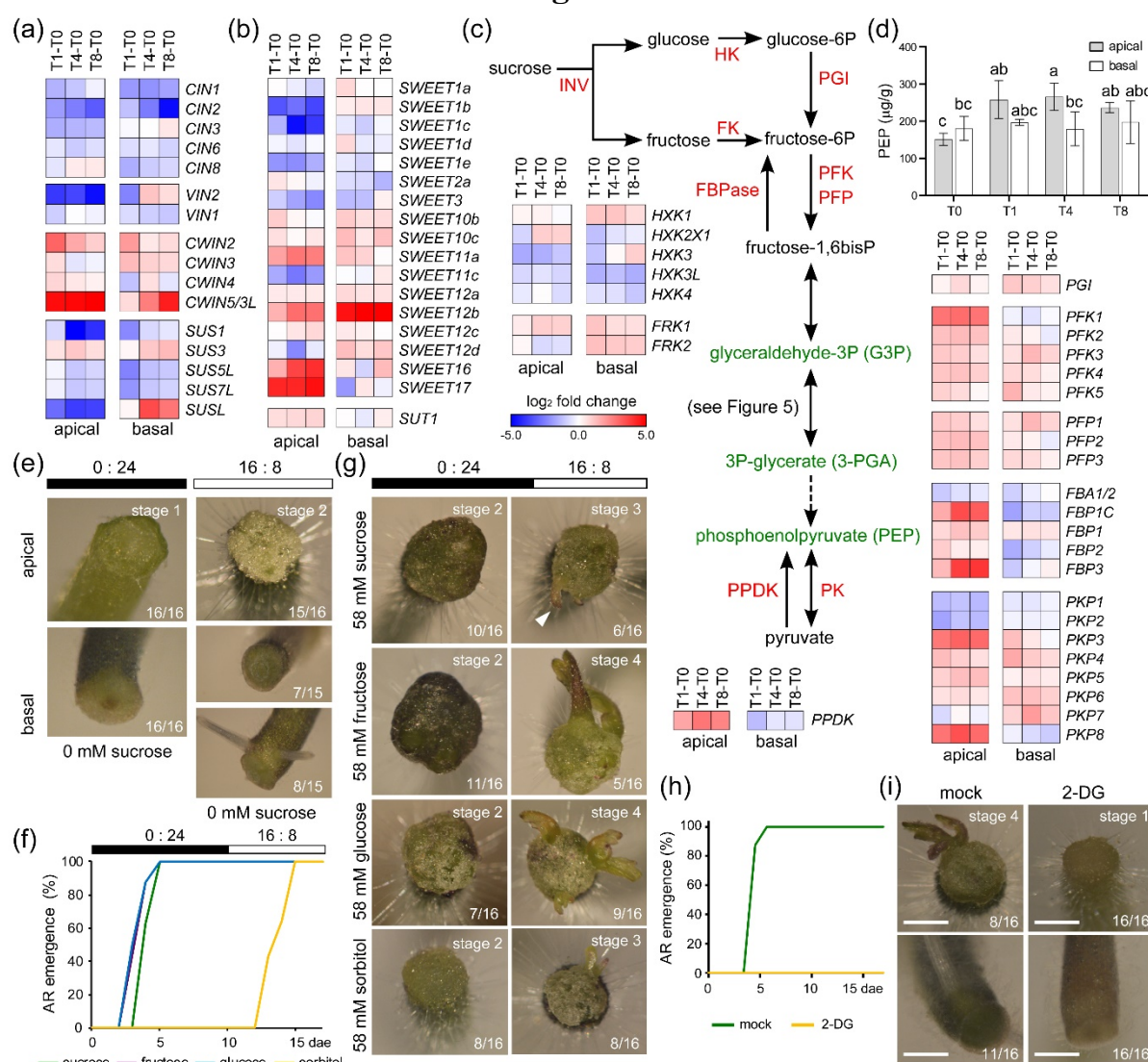
Figure 6

Figure 6. **Sucrose is required for wound-induced organ formation**. (a) DEG encoding invertases (CIN, VIN and CWIN) and sucrose synthases (SUS). (b) DEG encoding putative sugar transporters of the SWEET and SUT families. (c) Some DEG encoding enzymes in the glycolysis/gluconeogenesis pathway. Genes encoding the key enzymatic activities of the different steps in the pathway are shown: INV, invertase; HK, hexokinase; FK, fructokinase; PGI, phosphoglucose isomerase; PFK/PFP, phosphofructokinase; FBPase, fructose bisphosphatase; PK, pyruvate kinase; PPDK, pyruvate-phosphate dikinase. (d) Endogenous levels of phosphoenolpyruvate in the apical and basal region of the hypocotyl explants during the studied time-course. (e) Representative images of *de novo* organ formation in the apical and basal region of the hypocotyl explants on different photoperiod conditions (16:8 and 0:24) without sucrose. (f) AR emergence of hypocotyl explants grown for 10 days on 0:24 photoperiod followed by 7 days on 16:8 photoperiod. (g) Representative images of shoot formation stages in the apical region of the hypocotyl explants grown on different sugars with same photoperiod conditions as in (f). (h) Rooting capacity of hypocotyl explants at 14 dae on SGM (mock and 2-DG) and 16:8 photoperiod. Different letters (d, f, h) indicate significant differences (p-value<0.01) between the assayed conditions. (i) Representative images of *de novo* organ formation in the apical and the basal region of the hypocotyl explants on SGM (mock and 2-DG) and 16:8 photoperiod. Gene annotations (a-c) are found in Supplemental Tables 6 and 7. Scale bars (e, g, i): 1 mm.